



HAL
open science

The accuracy and precision of multi-line NO-LIF thermometry in a wide range of pressures and temperatures

Kae Ken Foo, Nathalie Lamoureux, Armelle Cessou, Corine Lacour, Pascale Desgroux

► **To cite this version:**

Kae Ken Foo, Nathalie Lamoureux, Armelle Cessou, Corine Lacour, Pascale Desgroux. The accuracy and precision of multi-line NO-LIF thermometry in a wide range of pressures and temperatures. *Journal of Quantitative Spectroscopy and Radiative Transfer*, 2020, 255, pp.107257. 10.1016/j.jqsrt.2020.107257 . hal-02997167

HAL Id: hal-02997167

<https://hal.science/hal-02997167>

Submitted on 9 Nov 2020

HAL is a multi-disciplinary open access archive for the deposit and dissemination of scientific research documents, whether they are published or not. The documents may come from teaching and research institutions in France or abroad, or from public or private research centers.

L'archive ouverte pluridisciplinaire **HAL**, est destinée au dépôt et à la diffusion de documents scientifiques de niveau recherche, publiés ou non, émanant des établissements d'enseignement et de recherche français ou étrangers, des laboratoires publics ou privés.

The accuracy and precision of multi-line NO-LIF thermometry in a wide range of pressures and temperatures

Kae Ken Foo^{a,*}, Nathalie Lamoureux^a, Armelle Cessou^b, Corine Lacour^b, Pascale Desgroux^a

^a*Univ. Lille, CNRS, UMR 8522 - PC2A - Physicochimie des Processus de Combustion et de l'Atmosphère, F-59000 Lille, France*

^b*CNRS UMR 6614 - CORIA - University of Rouen - Madrillet University Site - 675, avenue de l'Université BP 12 76801 SAINT ETIENNE DU ROUVRAY CEDEX*

Abstract

An automated spectral fitting algorithm (named Thermo NO-LIF) designed for the extraction of temperature information from experimental NO-LIF spectra is presented and analysed. With the aid of the Thermo NO-LIF, the high-accuracy (0.5%) of multi-line NO-LIF thermometry are demonstrated in the burnt-gases region of a near-adiabatic Bunsen-type premixed flame. The results are compared with the temperature measured using N₂ spontaneous Raman scattering (SRS). The current study also applies and analyses the algorithm and the thermometry technique in a premixed flat-flame under various sub-atmospheric pressures. The results suggest that choosing a long excitation scan range with as few overlapping lines as possible can maximise the performance of the multi-line NO-LIF thermometry. The uncertainty arising from the overlapping lines is especially crucial at atmospheric pressure. Additionally, the current study compares the performance of multi-line NO-LIF thermometry using narrowband and broadband lasers. Thermo NO-LIF is available to anyone interested in applying multi-line NO-LIF thermometry.

Keywords: Nitrogen oxide, laser-induced fluorescence, thermometry, MATLAB, temperature, methane flame

1. Introduction

Accurate determination of temperature is always of critical part in characterising reactive gaseous flow systems, where temperature plays a crucial role in physics and chemistry. In this context, various thermometry approaches based on laser-induced fluorescence (LIF) have been developed and widely applied in a broad range of combustion studies [1–6]. The principle of LIF thermometry relies on the temperature dependence of the population distribution of different rotational, vibrational or electronic energy levels of the target species. Either molecules (e.g. NO [4–6], OH [7, 8], CH, C₂ [9] and CN [1]) or atoms (e.g. indium [3, 10] and

* I am the corresponding author

gallium [11]) can be employed as fluorescence tracers. Among the molecular species, NO is a popular candidate due to several of its advantageous properties. Contrary to OH, CH, C₂, and CN, which are short-lived combustion intermediates present in limited regions of flames, NO is chemically stable at room temperature and elevated temperatures. Its stability allows the measurement of a wide range of temperature accessible to LIF thermometry. Although NO naturally occurs in most combustion systems, it is readily available for seeding if it is necessary to increase the signal-to-noise ratio (SNR). Furthermore, the fluorescence quantum yield of NO is independent of the rotational number [7, 12]. As a result, multi-line NO-LIF thermometry is applicable without corrections for quenching and radiative lifetime [13].

Multi-line NO-LIF thermometry relies on the probing of multiple ground states by tuning the laser over a range of excitation wavelengths [1, 4, 7]. It can be applied for either single-point or imaging measurements. The limitation of the technique is that it requires a data acquisition period longer than the timescales of turbulence and chemical reaction. Nonetheless, the technique has been applied in mildly turbulent flames to obtain temporally averaged temperatures [14, 15]. However, the temperature bias observed in the flame contour region, where the ambient air and burnt gases mix vigorously, could be as high as $\pm 25\%$. Despite its limitation, multi-line NO-LIF thermometry remains a robust and versatile tool that has wide applications in different fields, for example, nano-particles synthesis [16], plasma [17, 18], soot formation [19, 20], biofuels [6, 21] and evaporating spray systems [22].

There are multiple methods to extract temperature information from excitation scan spectra. The most straightforward approach is to plot the peak intensities of individual rotational line logarithmically against the corresponding rotational energy [1, 23]. The resultant Boltzmann plot gives a straight line with a slope $-1/(k_B \cdot T)$, where k_B is the Boltzmann's constant and T is the temperature. The Boltzmann plot method is insightful because any point deviates from the slope is easily detected and the goodness of the linear fit reflects the reliability of the temperature measurement. The determination of peak intensities is often done by selecting the local maxima of a spectrum. However, if there are not enough data points available to characterise the peaks precisely, a fitting procedure is required to obtain the local maxima which potentially introduces additional uncertainties. Additionally, if the instrumental resolution is broader than the spectral distance between the rotational lines, spectral overlaps are inevitable. Even partially overlapping spectra can lead to uncertainties in the Boltzmann plot method. In this context, the current study examines the impacts of laser spectral resolution on the accuracy and precision of multi-line NO-LIF thermometry using a frequency-doubled Nd:YAG-pumped dye laser with and without an injection seeding system, which provide narrowband and broadband lasers, respectively.

Alternatively, temperatures can be determined via spectral fitting. There are publicly available software packages that simulate spectra, for example, LIFBASE [24], LIFSim [25] and PGOPHER [26]. LIFSim offers a direct fitting function on its website, unfortunately, it lacks detailed documentation on how the fitting process works. It is still common to compare the experimental spectrum to a library of predetermined synthesised spectra to obtain the best-fitted temperature [6, 16, 19–22]. In general, the free parameters are temperature, baseline and signal intensity, with the lineshape parameters determined by comparing the experimental spectrum to simulated spectra [6, 19, 20]. The process is time-consuming

and subjective. The current study proposes a spectral fitting programme, named Thermo NO-LIF, that provides temperature by directly fitting the experimental spectrum; here, temperature, baseline, fluorescence intensity, linewidth, peak position are free parameters. However, it is necessary to fine-tune the peak position of each excitation line due to the experimental deficiency arising from the sine bar driven grating in the laser tuning system [1, 6, 27]. Contrary to LIFSim, where both the Gaussian and Lorentzian linewidths are fitted simultaneously, Thermo NO-LIF characterises the spectral lineshape using a pseudo-Voigt function where the convoluted linewidth and Lorentzian factor are fitted to the experimental spectra.

The accuracy and precision of determining temperature using Thermo NO-LIF are examined and analysed in a wide range of temperatures and pressures. Coherent anti-Stokes Raman scattering (CARS) is often used as a benchmark for the performance of temperature diagnostic techniques [4, 28] since it provides the highest accuracy among all thermometry techniques, especially with nitrogen as an indicator molecule [29–31]. Bessler and Schulz [4] have compared temperatures acquired using multi-line NO-LIF with those employed N₂-CARS and they agree to within ~ 150 K. The current study compares the measurements obtained with multi-line NO-LIF to those provided using N₂ spontaneous Raman scattering (SRS) [32] in the same CH₄/air Bunsen-type premixed laminar flame. N₂ SRS was chosen because it provides an absolute measurement of temperature without any calibration in a reference medium [33]. The current study applies multi-line NO-LIF thermometry in isothermal flow (~ 290 K), flat-flames at sub-atmospheric pressures (1.33–40 kPa) and an atmospheric Bunsen-type premixed flame (101.3 kPa). It examines the robustness of Thermo NO-LIF by employing broadband and narrowband lasers to excite different spectral ranges.

2. Experiment

2.1. Burners

Investigations carried out at sub-atmospheric pressures were conducted in a stainless steel enclosure (30 cm height and 24 cm diameter) connected to a vacuum pump. A bronze water-cooled McKenna burner with a diameter of 6 cm was placed inside the enclosure with the ability to translate vertically. The pressure inside the enclosure was monitored with a pressure transducer and was regulated using an automatic control valve. The pressure can be controlled to an accuracy of $\pm 1\%$.

The composition of the gas mixture was controlled using mass flow controllers of 1, 2 and 5 SLPM (with $\pm 0.5\%$ full-scale precision) for CH₄, O₂ and N₂, respectively. For room-temperature measurements, no flame was ignited and only N₂ seeded with 120 ppm of NO (2.002 mol% NO in N₂; $\pm 0.5\%$ full-scale precision) flowed through the enclosure. For flame temperature measurements, a laminar premixed flat-flame was established under pressures 4.0, 12.0, 24.0 and 40.0 kPa. The volumetric flow rates for CH₄, O₂ and N₂ were 0.533, 1.067 and 3.400 SLPM, respectively. Additionally, 120 ppm of NO was seeded into the cold fuel mixture, substituting N₂. Such an amount of NO provides a typical SNR of 65:1 without perturbing the flames.

Measurements at atmospheric pressure were performed in a Bunsen-type burner [32] that provides laminar, stable and well-characterised premixed flames. The current study conducted measurements in the same stoichiometric CH₄/air premixed flame that has been investigated previously in this burner with N₂ SRS [32]. Instead of using compressed air, the current study synthesised air with 21% of O₂ and 79% of N₂. The volumetric flow rates for CH₄, O₂ and N₂ are 0.857, 1.718 and 6.463 SLPM, respectively. The flame height was measured and compared with the previous study to confirm the reproducibility of the flame. Similar to the sub-atmospheric pressure flames, 120 ppm of NO was seeded into the cold fuel mixture, substituting N₂. Measurements were probed at a height above the burner (HAB) of 24 mm, in the burnt-gases region at the same location as in the SRS study [32]. It is where the flame temperature was found to be nearly adiabatic in this CH₄/air flame, due to the weak effect of curvature and heat-loss far from the tip and the burner lip.

2.2. Laser and optical setup

A frequency-doubled injection-seeded Nd:YAG laser (Quantel Q-smart 850) was utilised to pump a tunable dye laser (Quantel TDL+) that used a mixture of rhodamine 590 and rhodamine 610 dissolved in ethanol. The mixture ratio was adjusted such that the laser energy was optimised for operation around 572 nm. The dye laser emission was first frequency-doubled to 286 nm and then mixed with the residual fundamental beam of the Nd:YAG using non-linear crystals mounted in a tracking unit. As a result, it generated an ultra-violet (UV) beam at approximately 225 nm which is ideal for exciting the NO A-X(0,0) band. A motorised Pellin-Broca prism was utilised to isolate the desired wavelength without deviating the laser beam axis. The UV beam passed through an iris diaphragm and an attenuator in which the laser energy was limited to the linear LIF regime. The beam was shaped into a 1 × 5 mm sheet through a horizontal slit. For all measurements, the laser scan rate was 0.35 pm s⁻¹ and the signal was continuously averaged over seven laser pulses. The laser energy fluctuations were monitored with a photodiode after the sheet passed through the flames. The LIF signals were subsequently collected via a two-lens-system and focused onto the horizontal entrance slit of a 500 mm focal length monochromator with a 1200 mm⁻¹, 300 nm blaze wavelength grating. To compensate for the low local density of NO at sub-atmospheric pressures, the entrance slit of the monochromator was 0.25 × 10 mm for experiments conducted in the flat-flame. In contrast, it was reduced to 0.25 × 4 mm for measurements at atmospheric pressure to obtain a spatial resolution adequate to the flame region in which the temperature was found homogenous. Previous measurements performed using Raman spectroscopy [32] showed that T was homogeneous up to a radius of 6 mm at HAB probed in the current study. The monochromator was adjusted to provide an output with a ~10 nm spectral width around a centre wavelength of 245 nm to obtain the fluorescence signals in the entire vibrational band of NO A-X(0,2). It was chosen to avoid the interference from hot O₂ fluorescence [34]. The fluorescence signals were collected with a photomultiplier tube (Photonis XP2020Q). The fluorescence and laser intensity signals were simultaneously gathered and recorded via an oscilloscope (LECROY 9354A, 8-bit vertical resolution, 500 MHz bandwidth, 1 GS s⁻¹).

The choice of NO transitions is of importance for high-quality performance of multi-line NO-LIF thermometry. The current study selected several spectral ranges in the literature and analysed their performance at various temperatures and pressures. Numerical analyses conducted by Bessler and Schulz [4] suggested that, within the NO A-X(0,0) band, simulated excitation scans in the spectral range 44300–44 400 cm^{-1} exhibit high temperature-sensitivity at 500 and 2000 K. They then proposed four shorter scan ranges: (a) 44376–44 381 cm^{-1} , (b) 44376–44 386 cm^{-1} , (c) 44407–44 417 cm^{-1} , and (d) 44402–44 417 cm^{-1} . Among these, the scan range 44407–44 417 cm^{-1} exhibited the overall best performance [4]. One of the proposed scan ranges, (b), coincides with the one derived from a previous study [5], which is 44375–44 385 cm^{-1} . Both scan ranges are comparable although the latter one differs from the prior one by 1 cm^{-1} .

In previous studies [6, 12], the authors employed a scan range 44306–44 352 cm^{-1} following the work of Hartlieb et al. [7]. To determine the optimum excitation spectral range within the NO A-X(0,0) band, the current study examined scan ranges 44306–44 352 cm^{-1} and 44375–44 417 cm^{-1} which includes the short scan ranges suggested by Bessler and Schulz [4] and utilised by Denisov et al. [5]. Additionally, experiments were also conducted at constant room temperature, but under systematically varied sub-atmospheric pressures. The objective was to study the practicality of Thermo NO-LIF against line broadening while isolating the collisional effect from the Doppler effect. To increase the temperature sensitivity at room temperature, the current study employed another scan range, 44195–44 232 cm^{-1} , that included lower rotational quantum number transitions for room-temperature measurements. The ambient temperature was measured to be 290 K using a type K thermocouple. Table 1 summarises the excitation ranges employed in the current study while each scan range is assigned a symbol.

Table 1: Summary of the excitation ranges employed in the current study.

Symbol	Excitation range	Amount of peaks	Reference
A	44375–44 417 cm^{-1}	16	
A ₁	44376–44 381 cm^{-1}	4	[4]
A ₂	44376–44 386 cm^{-1}	6	[4] and [5]
A ₃	44407–44 417 cm^{-1}	5	[4]
A ₄	44402–44 417 cm^{-1}	4	[4]
B	44303–44 353 cm^{-1}	22	[6, 7]
B ₁ ^a	44303–44 341 cm^{-1}	17	
C ^b	44195–44 232 cm^{-1}	23	

^a To reduce the amount of overlapping lines.

^b Utilised for room-temperature measurements only as it includes transitions with lower rotational numbers.

2.3. Spectral fitting programme Thermo NO-LIF

Thermo NO-LIF was built in-house using MATLAB[®] R2019a. It directly fits the experimental NO-LIF spectra to an equation that relates the LIF intensity to the rotational

temperature. This section discusses the principle and procedures involved in the algorithm.

The LIF intensity and the line profile are the two essential constituents of an excitation spectrum. The LIF intensity, I_i , of the i^{th} transition can be characterised as follows [35]:

$$I_i \propto N_0 \cdot I_L \cdot g_\nu \cdot B_i \cdot f_{Bi} \cdot \frac{A_i}{\sum_i A_i + k_p + k_q} \quad (1)$$

where N_0 is the total number density, I_L is the incident laser intensity, g_ν represents the spectral overlap of the laser profile and the absorption line, B_i is the Einstein absorption coefficient obtained from LIFBASE [24] and f_{Bi} is the Boltzmann fraction of the initial level. The last term is to describe the fluorescence quantum yield which depends on the Einstein emission coefficient, A_i , divided by the sum of A_i over all vibrational states plus predissociation rate, k_p , and quenching rate, k_q . This equation is only valid if I_L is maintained in the linear LIF regime.

A few modifications are required to simplify Eq 1. Firstly, N_0 is omitted in the following equations because, throughout an excitation scan, the total number density of NO within the probed volume is constant in steady flames. Secondly, the fluorescence quantum yield of NO is neglected since it is independent of the rotational number [7]. Lastly, f_{Bi} can be expressed as a function of T :

$$f_{Bi} = \frac{(2J_i + 1)}{Q_{vib} \cdot Q_{rot} \cdot Q_{elec}} \cdot e^{-\frac{E(J_i)}{k_B \cdot T}} \quad (2)$$

where $(2J_i + 1)$ is the degeneracy of the rotational state and J_i is the rotational quantum number of lower state of i^{th} transition. Q_{vib} , Q_{rot} and Q_{elec} are the vibrational, rotational and electronic partitions calculated numerically. The energy of the rotational state, $E(J_i)$ is calculated following the equations and spectroscopic constants provided by Reisel et al. [36]. The energies for rotational level J_i are given by

$$E(J_i) = B_v'' \cdot [(J_i + 0.5)^2 - 1] - D_v'' \cdot [(J_i + 0.5)^4 - (J_i + 0.5)^2 + 1] \mp B_v'' \cdot \sqrt{\alpha}, \quad (3)$$

where

$$\alpha = \frac{(Y_v - 2)^2}{4} + [(J_i + 0.5)^2 - 1] \cdot (1 + 2 \cdot \mu \cdot [2 \cdot (J_i + 0.5)^2 - Y_v] + \mu^2 \cdot ([2 \cdot (J_i + 0.5)^2 - 1]^2 - 1)), \quad (4)$$

$$Y_v = \frac{A \pm C \cdot (J_i - 0.5)^2}{B_v''}, \quad (5)$$

$$\mu = \frac{D_v''}{B_v''}. \quad (6)$$

Here, B_v'' is the rotational constant, D_v'' is the centrifugal stretching of the molecule, A is the spin-splitting term, and C is an additional term accounting for spin-splitting in the

Table 2: Spectroscopic constants for NO A-X(0,0) band taken from Reisel et al. [36].

Constant	Value (cm ⁻¹)
B''_v	1.696190
D''_v	5.326×10^{-6}
A	123.0372
C	-1.1871×10^{-3}

rotational energy. The symbols \mp and \pm are used to distinguish between the ${}^2\Pi_{1/2}$ state, where the upper signs should be used, and the ${}^2\Pi_{3/2}$ state, where the lower signs should be used. Table 2 lists the spectroscopic constants used in the current study for the NO A-X(0,0) band.

Excluding those rotational-independent parameters, Eq. (1) can be reduced to

$$I_i \propto I_L \cdot g_\nu \cdot B_i \cdot (2J_i + 1) \cdot e^{-\frac{E(J_i)}{k_B T}}. \quad (7)$$

Here, I_i can be normalised through dividing the LIF excitation spectrum using the temporal energy profile of the incident laser. Additionally, the spectral lineshape g_ν is best described using a convolution integral of Gaussian and Lorentzian functions, known as the Voigt profile [37] :

$$V(\nu) = G(\nu) \otimes L(\nu) = \int_{-\infty}^{\infty} G(\nu') \cdot L(\nu - \nu') \cdot d\nu'. \quad (8)$$

Here, $G(\nu)$ is the Gaussian function

$$G(\nu) = \exp \left[-4 \cdot \ln 2 \cdot \left(\frac{\nu - \hat{\nu}}{\Gamma_G} \right)^2 \right] \quad (9)$$

and $L(\nu)$ is the Lorentzian function

$$L(\nu) = \left[1 + 4 \cdot \left(\frac{\nu - \hat{\nu}}{\Gamma_L} \right)^2 \right]^{-1}, \quad (10)$$

where ν is wavenumber in unit cm⁻¹, $\hat{\nu}$ is the spectral position of the peak intensity obtained from LIFBASE [24], Γ_G and Γ_L are the Gauss and Lorentz full-width at half maximum (FWHM), respectively. Since the Voigt function cannot be expressed in finite terms of elementary functions [38], for computational purposes, various alternate approaches [39–42] have been proposed in an attempt to analytically approximate the complex function. Schreier [38, 43, 44] has extensively reviewed this subject. The Voigt function is a powerful tool that has important applications in many fields of science. Thus, most of the approximations are limited to solve specialised problems. The current study, therefore, selects one of

the simplest approximation, the summation of $G(\nu)$ and $L(\nu)$, also known as pseudo-Voigt function:

$$V_p(\nu) = (1 - \eta) \cdot \exp \left[-4 \cdot \ln 2 \cdot \left(\frac{\nu - \hat{\nu}}{\Gamma_V} \right)^2 \right] + \eta \cdot \left[1 + 4 \cdot \left(\frac{\nu - \hat{\nu}}{\Gamma_V} \right)^2 \right]^{-1}, \quad (11)$$

where η is Lorentzian weight factor. Instead of fitting both Γ_G and Γ_L as done in the previous study [27], here, only the convoluted linewidth Γ_V is being considered, assuming $\Gamma_V = \Gamma_G = \Gamma_L$. This provides an approximation accurate to $\sim 1\%$ [45, 46]. Furthermore, Jain et al. [40] demonstrated that the summation of $G(\nu)$ and $L(\nu)$ is a better approximation of the Voigt function than the product of $G(\nu)$ and $L(\nu)$. Both the Doppler and collisional broadening components can be deduced using the following equations (accurate to 0.02%) [47]:

$$\Gamma_V = \frac{1}{2} \left(1.0692 \cdot \Gamma_c + \sqrt{0.8664 \cdot \Gamma_c^2 + 4(\Gamma_D^2 + \Gamma_I^2)} \right), \quad (12)$$

where the collisional broadening, Γ_c , is given by [48],

$$\Gamma_c = 0.585 \left(\frac{P}{101.325} \right) \left(\frac{300}{T} \right)^{0.75} \quad (13)$$

and the Doppler broadening is given by the general expression

$$\Gamma_D = 7.16 \times 10^{-7} \cdot \bar{\nu} \cdot \sqrt{\frac{T}{M}}, \quad (14)$$

where P is pressure in unit kPa, $\bar{\nu}$ is the centre wavenumber of the excitation range in unit cm^{-1} . M is the molar mass of NO, 30.01 g mol^{-1} . Here, instead of measuring Γ_I , the value is inferred by calculation using Eq. 12.

By combining Eqs. (7) and (11) with a constant background c , the synthesised spectrum, $S(\nu)$, can be expressed as:

$$S(\nu) = c + \sum_i B_i \cdot (2J_i + 1) \cdot e^{-\frac{E(J_i)}{k_B \cdot T}} \cdot \left((1 - \eta) \cdot \exp \left[-4 \cdot \ln 2 \cdot \left(\frac{\nu - \hat{\nu}}{\Gamma} \right)^2 \right] + \eta \cdot \left[1 + 4 \cdot \left(\frac{\nu - \hat{\nu}}{\Gamma} \right)^2 \right]^{-1} \right). \quad (15)$$

To solve $S(\nu)$, the spectroscopic constants are available in the literature for NO. Thus, it is expected that Thermo NO-LIF possesses the potential to fit excitation spectra of other fluorescence species, provided that the spectroscopic parameters of the species are known. The fitting parameters are T , η , Γ , $\hat{\nu}$ and c . It is necessary to fit $\hat{\nu}$ because, as aforementioned,

the spectral positions of the experimental and simulated transitions do not match exactly even after fine-tuning the experimental spectrum. This approach further eliminates the errors introduced by the uncertainty in spectral positions.

To perform the fitting process, both the experimental spectrum and Eq. (15) must be normalised to the same order of magnitude, usually unity. The conventional way to normalise a spectrum is to divide the total spectrum with the maximum intensity. However, it is impossible to obtain maximum intensity without constructing the whole spectrum. Hence, Eq. (15) is required to be divided with a temperature-dependent normalisation term. One of the approaches is to construct a library of simulated spectra that has the same spectral range as the examined experimental spectrum. Then, it extracts the maximum theoretical fluorescence intensity, corresponding to the experimental ones, as a function of temperature. The non-linear function is fitted with a Fourier series.

Figure 1 shows the convergences of the best-fitted T ((a) and (c)) and Γ_V ((b) and (d)) for fitting processes using a temperature-dependent normalisation term (solid line) and using a free-fitting normalisation term as done in LIFSim [27] (dashed line). The fitting processes were executed using the same bounds and start points (300 and 2000 K for room-temperature and near-adiabatic flame temperature measurements, respectively). It is clear that using a temperature-dependent normalisation term, the best-fitted temperature converged (≤ 250 iterations) ten times faster than that of the case where a free-fitting normalisation parameter was used (≥ 2500 iterations). In addition to facilitating the fitting process, this approach also enhances the consistency between different evaluations.

3. Results and Discussion

3.1. Collisional and Doppler broadening

Figure 2 shows examples of experimental and fitted spectra of NO-LIF acquired under the pressure of 40 kPa with the narrowband laser. The NO-LIF spectra in panels (a) and (b) were obtained in the burnt-gases region (HAB=20 mm) of a premixed flat-flame. Temperatures derived from the spectra (a) and (b) are 1599 K and 1556 K, respectively. In contrast, the spectrum in panel (c) was collected at room temperature where the best-fitted temperature is 293 K. Additionally, the shorter ranges in scan ranges A and B are shown as marked by their symbols. Since Γ_c is inversely proportional to T , high temperatures have a counter-effect on the collisional broadening. As a result, spectrum C exhibits a more Lorentzian appearance compared with the other two spectra. Moreover, the calculations using Eqs. (12), (13) and (14) show that the total line broadening at 293 K is 0.28 cm^{-1} , which is slightly higher than the values obtained at 1599 and 1556 K, 0.26 cm^{-1} .

3.2. Room-temperature measurements

It can be seen from Eq. (15) that while both the fluorescence intensity term and the lineshape profile are directly or indirectly related to the temperature, they are independent of each other. Therefore, although the laser linewidth is not sufficiently narrow to accurately

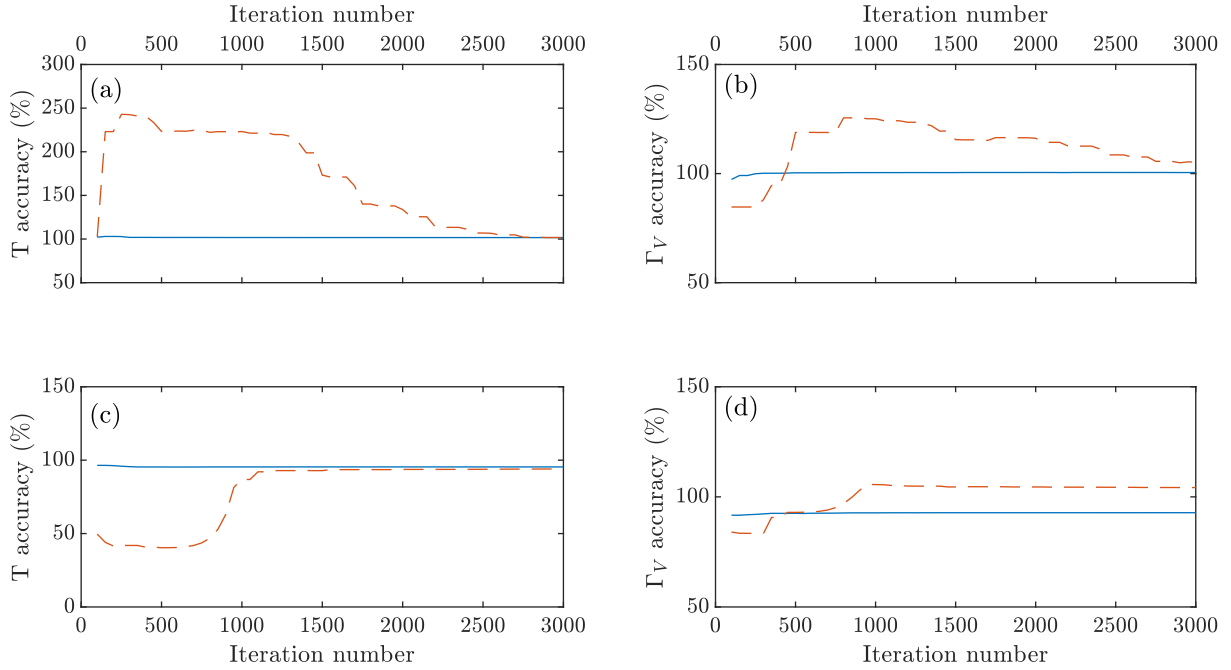


Figure 1: Convergence of the best-fitted temperature, T , and linewidth, Γ_V , as functions of the iteration number, for measurements (a) and (b) conducted at room-temperature (293 K; 20 kPa); (c) and (d) in the near-adiabatic Bunsen-type flame (2145 K; 101.3 kPa). The solid line represents the convergence using a temperature-dependent normalisation term. The dashed line represents the convergence using a free-fitting normalisation term.

determine the temperature [1], the best-fitted linewidth can be employed as an alternate confirmation tool for the temperature measurements by comparing it with its theoretical counterpart based on the best-fitted temperature. To accurately predict the theoretical spectral linewidth at any pressure and temperature, the information of Γ_I is essential. Hence, the room-temperature measurements were conducted where both the pressure and temperature were known to the accuracy of 1% (the accuracies of the pressure gauge and the type K thermocouple).

Table 3 shows the best-fitted temperature of spectra within scan range C collected at room-temperature N_2 gas flow with seeded NO at various sub-atmospheric pressures and the best-fitted Voigt linewidth, Γ_V , with its theoretical counterpart, $\Gamma_{V,theo}$. The temperature average is 285 ± 8 K, which agrees with the thermocouple measured temperature, 290 ± 3 K. Only one spectrum was collected at each pressure, hence, only the accuracy is presented in the table. Fig. 3 plots Γ_V and $\Gamma_{V,theo}$ as functions of P to deduce the instrumental linewidth, Γ_I . The y-intercept is assumed to be the convolution between Γ_I and Γ_V , isolated from Γ_c where $P = 0$ kPa. Using Eq (12), Γ_I is calculated to be 0.12 cm^{-1} while Γ_D is 0.10 cm^{-1} . $\Gamma_{V,theo}$ is estimated based on the derived Γ_I and the theoretical collisional and Doppler broadening. The plot shows that the largest disagreement occurs at the measurement at 24.0 kPa, which is 3.1% lower than the thermocouple measurement, while the best-fitted Γ_V agrees with the theoretical value to within 5%. In contrast, the largest discrepancy be-

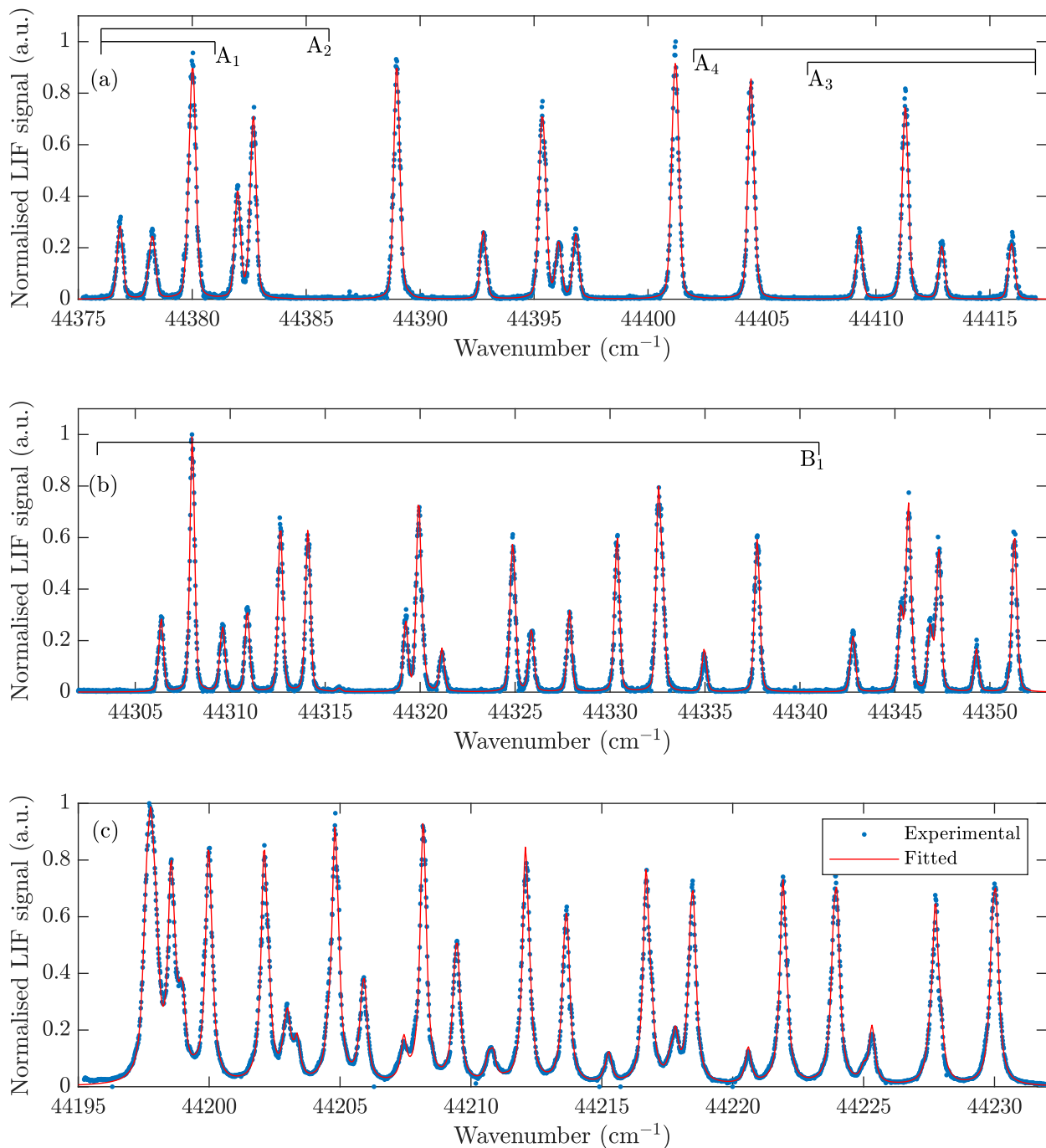


Figure 2: Examples of fitted experimental spectra collected at 40 kPa and (a) 1599 K within scan range A, (b) 1556 K within scan range B, and (c) 293 K within scan range C. Shorter scan ranges within A and B are shown as well.

tween the best-fitted and theoretical linewidths occurs at 36.0 kPa, up to 16%. Nevertheless, the accuracy of the temperature measurement under this pressure is better, 1.7%. Despite the individual large discrepancy, the overall agreement between the best-fitted and esti-

mated linewidths is within 8%. This is consistent with Rensberger et al. [1] who concluded that the fitting of temperature is not highly dependent on the linewidth. Nevertheless, it still serves as an indicator. Furthermore, the gradients of both linear fits agree with each other to within 2%, indicating that the collisional broadening component of the best-fitted linewidths can be well-characterised using the collisional-broadening coefficient derived by Chang et al. [48]. This improves the confidence in using the fitting programme to derive temperature measurements.

Table 3: Best-fitted temperatures, T , and linewidths, Γ_V , for spectra collected using a narrowband laser at different sub-atmospheric pressures, P . The theoretical linewidths, $\Gamma_{V,theo}$, are presented for comparison. The relative differences between the best-fitted temperatures and the thermocouple measured temperature are represented with ΔT .

P (kPa)	T (K)	ΔT	Γ_V (cm^{-1})	$\Gamma_{V,theo}$ (cm^{-1})
1.3	289	-0.3%	0.17	0.16
4.0	284	-2.1%	0.16	0.17
8.0	289	-0.3%	0.20	0.18
12.0	286	-1.4%	0.21	0.19
16.0	292	0.7%	0.22	0.21
20.0	295	1.7%	0.23	0.23
24.0	281	-3.1%	0.25	0.24
28.0	284	-2.1%	0.26	0.26
32.0	284	-1.4%	0.26	0.27
36.0	285	1.7%	0.24	0.29
40.0	293	1.0%	0.28	0.31

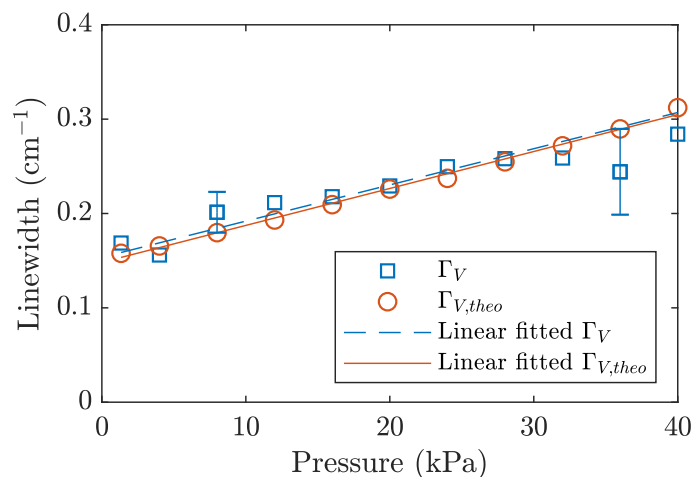


Figure 3: Best-fitted experimental and theoretical linewidths as function of pressures range from 1.3 to 40 kPa.

3.3. Near-adiabatic flame temperature measurements at atmospheric pressure

Instead of the room-temperature, measurements of elevated temperatures are where the interest lies. Hence, the current study assesses the accuracy and precision of multi-line NO-LIF associated with the proposed fitting algorithm via performing measurement in the burnt-gases region of a stoichiometric CH₄/air premixed Bunsen-type flame. The measurements are compared with those provided by Guichard et al. [32] and a computationally estimated adiabatic flame temperature, $T_{ad}=2145$ K. Table 4 presents the best-fitted temperatures, averaged over three spectra, the corresponding standard deviation, σ_T , and accuracy, ΔT , of each excitation scan range. Spectra B provide an average temperature of 2142 K which agree excellently with $T_{N_2} = 2134 \pm 55$ K (averaged over 400 single-shot measurements) and $T_{ad}=2145$ K. The average temperature derived from spectra A is approximately 4% lower than the adiabatic flame temperature. However, spectra B exhibit a σ_T significantly larger than that of spectra A. The results show that, by narrowing the excitation spectra to 44303–44341 cm⁻¹ (B₁), excluding the overlapping lines, R2(22)+Q1(24)+Q21(24) and P1(32)+Q2(28)+Q12(28), σ_T is halved while the accuracy is unaffected.

Unfortunately, it is not always possible to employ a long scan range due to the fluctuating nature of the system or the stability of the experiment over a long period of time. In this context, Table 4 also presents the averaged temperatures, the corresponding σ_T and ΔT evaluated for narrower scan ranges A₁, A₂, A₃ and A₄, following a previous study [4]. While Bessler and Schulz [4] examined the accuracy and precision of their fitting algorithm using LIFSim corrupted with artificial noise, the current study assesses the issue using experimental LIF signals. As expected, shorter scan ranges, except A₂, exhibit larger standard deviations than that of the long scan range A. The increase in standard deviation is not significant, except for the 10 cm⁻¹ scan range, A₃, where the standard deviation is 6.5%, five times more than that of the scan range A. Accuracy-wise, the 5 cm⁻¹ scan range, A₁, yields the best result. However, the scan range that provides the overall best performance in the previous study [4], A₃, does not perform well in these measurements. Nevertheless, the worst accuracy ($\Delta T = 7.2\%$) is still better than the absolute accuracy ($\Delta T = 8.0\%$) determined in the previous study [4]. The results imply that more than three short-range (approximately 10 cm⁻¹) spectra are required to yield a mean temperature that has a comparable accuracy and precision that a 38 cm⁻¹-long excitation scan B₁ provides.

Table 4: Best-fitted temperatures (averaged over three scans), \bar{T} , the standard deviation, σ_T , and the accuracy, ΔT (compared with $T_{ad} = 2145$ K), for NO-LIF spectra collected in the burnt-gases region of a CH₄/air premixed Bunsen-type flame.

Symbol	Scan range (cm ⁻¹)	\bar{T} (K)	σ_T	ΔT
A	42	2063	1.3%	-3.8%
A ₁	5	2090	1.5%	-2.6%
A ₂	10	1993	0.2%	-7.0%
A ₃	10	1990	6.5%	-7.2%
A ₄	15	2041	4.2%	-4.9%
B	50	2142	7.8%	-0.1%
B ₁	38	2143	3.8%	-0.1%

3.4. Flame temperature measurements at sub-atmospheric pressures

Table 5 presents the best-fitted temperatures extracted from LIF spectra excited using the narrowband laser in a premixed flat-flame across a wide range of sub-atmospheric pressures: 4.0, 12.0, 24.0 and 40.0 kPa. It compares the mean temperatures (averaged over three scans) and standard deviations σ_T , derived from spectra A, B, B₁, A₁, A₂, A₃ and A₄. In the absence of a reference temperature, the current study does not evaluate the accuracy of measurements at sub-atmospheric pressures. Instead, the current study compares the best-fitted temperatures derived from the scan range A with the mean temperature, \bar{T}_{A1-4} , averaged over those shorter scan ranges, A₁, A₂, A₃ and A₄. The dispersion in the temperatures derived from the short scan ranges is quantified by the standard deviation, σ_{A1-4} . The results show that the temperature gradually decreases as the pressure increases. It is due to the increased heat dissipation through the burner because the flame front is closer to the burner surface as the pressure increases.

The mean temperatures \bar{T}_{A1-4} obtained at different pressures agree with the best-fitted temperatures derived from long scan A to within 25 K, except for those acquired at 4.0 kPa. The dispersions in temperatures among the short scan ranges are also lower than that at 4.0 kPa. This indicates that there is a low-pressure threshold where the uncertainty increases significantly if it is crossed. The analysis shows that it might be related to the narrow linewidth of the excitation spectrum collected at these low-pressure ranges. The potential reason of this effect is discussed in § 3.5.

In contrast with the results obtained in atmospheric Bunsen-type premixed flame, excitation scan obtained with the spectral ranges B and B₁ do not show much difference in performance. The best-fitted temperatures obtained from both scan ranges agree with each other to within 22 K. Furthermore, excluding the overlapping lines does not lead to any significant improvement in σ_T . This indicates that at sub-atmospheric pressures, where the collisional broadening effect is not as severe as it is at atmospheric pressure, the uncertainty arising from the overlapping lines can be neglected.

3.5. Narrowband and broadband lasers

Figure 4 presents NO-LIF spectra within scan range B acquired in the atmospheric stoichiometric CH₄/air premixed Bunsen-type flame with (a) narrowband and (b) broadband lasers. The instrumental linewidths for the narrowband and broadband lasers are 0.12 and 0.68 cm⁻¹, respectively. Under atmospheric pressure, even though the collisional broadening is reduced significantly by the high temperature, the spectral resolution of the broadband laser remains too broad to resolve most of the adjacent transitions within this range. For example, the three peaks in the vicinity of 44 320 cm⁻¹ (indicated by arrows) are indistinguishable using a broadband laser. Furthermore, due to spectral overlapping, it is more challenging to identify the baseline using a broadband laser than a narrowband laser.

Table 6 presents the best-fitted temperatures extracted from the corresponding narrow- and broad-line-width spectra. Interestingly, NO-LIF spectra performed with a broadband laser provides similar results as those using a narrowband laser. Both narrow- and broad-line-width spectra give a better performance if scan range B₁ is used rather than the longer scan range B. To confirm whether this observation is consistent with the results obtained under lower pressures, the current study also performs a similar investigation at 5.3 kPa.

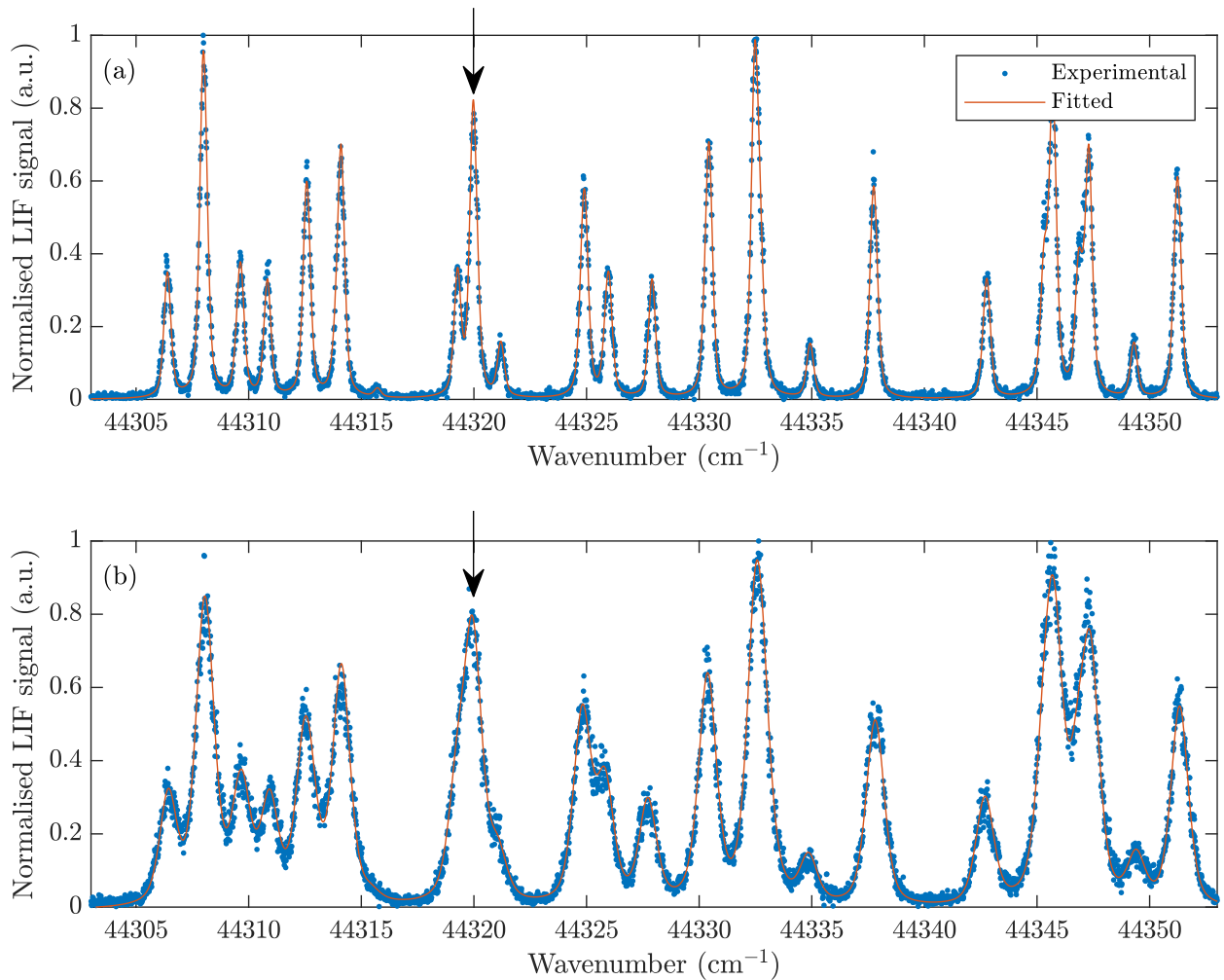


Figure 4: Examples of fitted experimental spectra (scan range B) collected in the burnt-gases region, HAB=24 mm, of the atmospheric stoichiometric CH₄/air premixed Bunsen-type flame using (a) narrow-band and (b) broadband lasers. The vertical arrow points out the three fluorescence peaks which are merged into a single peak due to the broader laser linewidth.

Figure 5 presents NO-LIF spectra obtained in a stoichiometric CH₄/O₂/N₂ premixed flat-flame stabilised at 5.3 kPa using (a) narrowband and (b) broadband lasers. In contrast to Fig. 4(a), the spectrum collected at 5.3 kPa (see Fig 5(a)) shows more experimental data which deviate from the fitting curve and most of them occurs at the peaks. Figure 6 shows the residuals from the spectral fit of the spectra collected at 5.3 and 101.3 kPa. For clarity, only every fifth residual in the spectral range of 44305–44 315 cm⁻¹ is shown. It is clear that the spectrum collected at 5.3 kPa exhibits more residuals compared with that obtained at atmospheric pressure (101.3 kPa). It appears that the narrowness of the spectral linewidth, which is the result of low pressure, affects the fitting algorithm. At 5.3 kPa, several peaks are so narrow that the height of the peak becomes ambiguous to the fitting algorithm. The issue is aggravated by the uncertainty in the spectral position due to the imperfection possessed by

the sine bar mechanism employed in the TDL system. This phenomenon indicates that extra care must be taken when performing the multi-line NO-LIF thermometry in low-pressure flames using narrowband lasers.

Table 7 presents the best-fitted temperatures derived from both the narrow- and broad-linewidth spectra. In the absence of a reference temperature, the accuracy of measurements at sub-atmospheric pressures remains undetermined. The values of \bar{T} do not differ much despite the scan range and the laser linewidth. However, σ_T increases significantly with the decrease in the scan range. This trend is the opposite of that observed in the results acquired at atmospheric pressure. It is most likely that the uncertainty introduced by the overlapping lines, R2(22)+Q1(24)+Q21(24) and P1(32)+Q2(28)+Q12(28), is nullified because they are well resolved at low pressures. It appears that at sub-atmospheric pressures, it is better to employ a longer scan range in performing the multi-line NO-LIF thermometry.

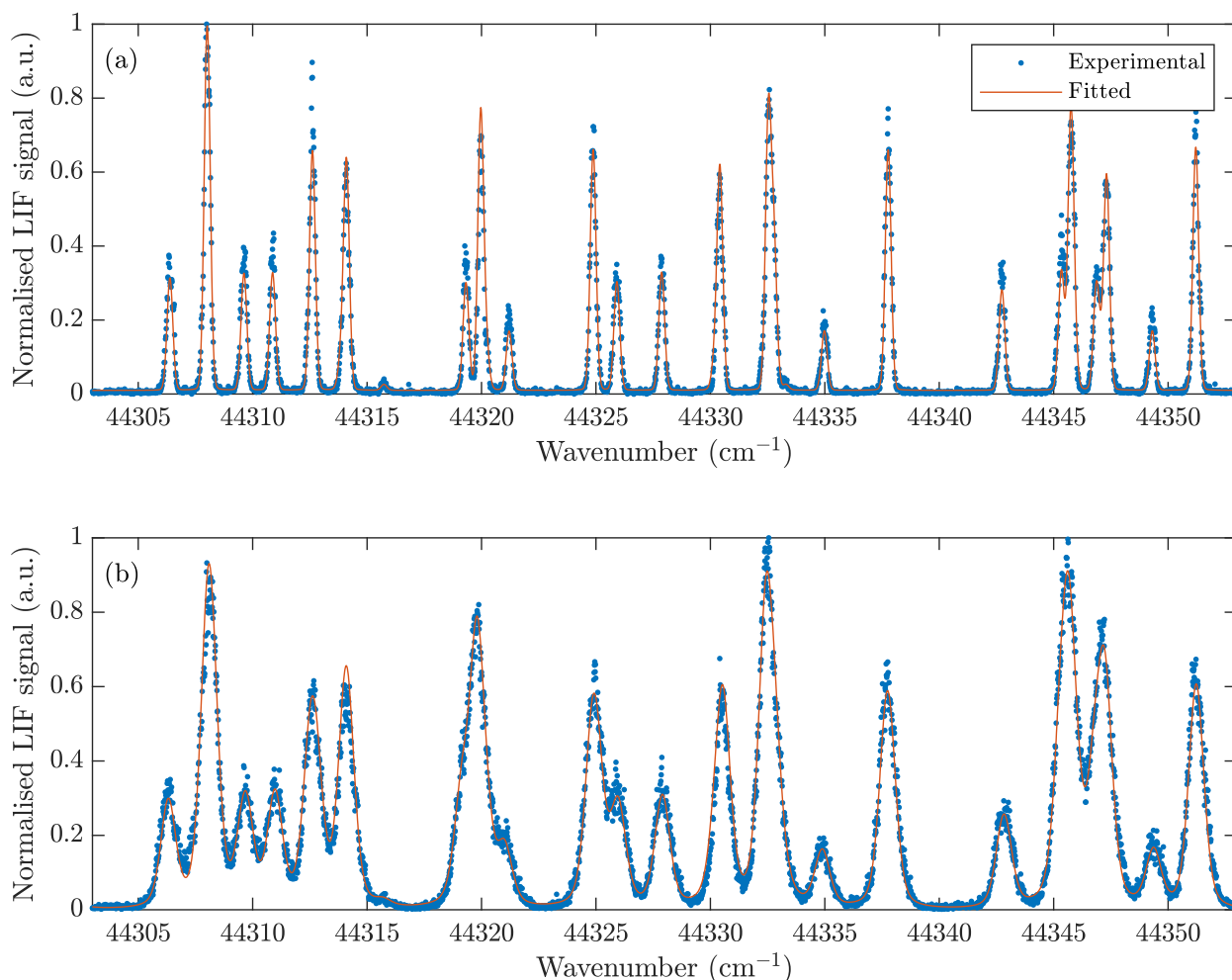


Figure 5: Examples of fitted experimental spectra (scan range B) collected in the burnt-gases region, HAB=25 mm, of the stoichiometric CH₄/O₂/N₂ premixed flat-flame under 5.3 kPa using (a) narrowband and (b) broadband lasers.

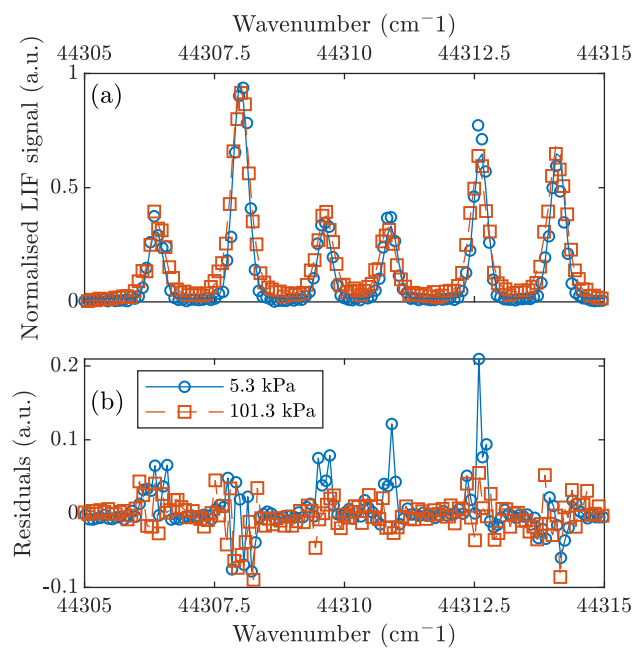


Figure 6: (a) Comparison of the experimental data and the best-fitted curves between spectra collected at 5.3 and 101.3 kPa using a narrowband laser. (b) Residuals from the spectral fit of the spectra within scan range B collected at 5.3 and 101.3 kPa. For clarity, only every fifth residual in the spectral range of 44305–44 315 cm^{-1} is shown.

Table 5: Temperature measurements performed in the burnt-gases region, $HAB = 20$ mm, of a premixed flat-flame at sub-atmospheric pressures: 4.0, 12.0, 24.0, 40.0 kPa using the narrowband laser. In addition, the mean temperature, \bar{T}_{A1-4} , averaged over different short scan ranges A_1 , A_2 , A_3 and A_4 is shown together with its standard deviation, σ_{A1-4} .

P (kPa)	Symbol	\bar{T} (K)	σ_T	\bar{T}_{A1-4} (K)	σ_{A1-4}
4.0	A	1813	1.0%		
	A ₁	1922	3.9%		
	A ₂	1687	8.7%	1761	9.4%
	A ₃	1868	4.0%		
	A ₄	1565	12.1%		
	B	1745	1.9%		
	B ₁	1739	3.7%		
	12.0	A	1625	2.1%	
A ₁		1644	4.3%		
A ₂		1617	11.5%	1660	2.5%
A ₃		1718	1.8%		
A ₄		1661	5.5%		
B		1734	2.1%		
B ₁		1736	2.4%		
24.0		A	1640	4.3%	
	A ₁	1620	3.8%		
	A ₂	1548	5.5%	1627	3.9%
	A ₃	1705	4.3%		
	A ₄	1636	5.1%		
	B	1613	1.9%		
	B ₁	1628	0.8%		
	40.0	A	1571	1.7%	
A ₁		1598	1.4%		
A ₂		1550	0.6%	1550	3.7%
A ₃		1583	3.0%		
A ₄		1470	6.3%		
B		1612	3.0%		
B ₁		1590	2.6%		

Table 6: Temperature and linewidth measurements performed with narrowband and broadband lasers in the stoichiometric CH₄/air premixed Bunsen-type flame. Additionally, the standard deviation σ_T and the accuracy ΔT are presented.

Laser linewidth	Symbol	Scan range (cm ⁻¹)	\bar{T} (K)	σ_T	ΔT
Narrowband	B	50	2142	7.8%	-0.1%
	B ₁	38	2143	3.8%	-0.1%
Broadband	B	50	2184	7.0%	1.4%
	B ₁	38	2174	4.5%	0.9%

Table 7: Temperature and linewidth measurements performed with narrowband and broadband lasers in the stoichiometric CH₄/O₂/N₂ premixed flat-flame under 5.3 kPa, along with the standard deviation σ_T .

Laser linewidth	Symbol	Scan range (cm ⁻¹)	\bar{T} (K)	σ_T
Narrowband	B	50	1727	1.4%
	B ₁	38	1685	2.8%
Broadband	B	50	1716	0.3%
	B ₁	38	1719	4.8%

4. Conclusions

A new spectral fitting programme, named Thermo NO-LIF, for multi-line NO-LIF within the A-X(0,0) band was applied and analysed in a wide range of temperatures and pressures. The programme automates the fitting process providing a consistent approach to evaluate NO-LIF spectra and derive temperature measurements without artefactual contributions. A series of experiments were performed in sub-atmospheric CH₄/O₂/N₂ premixed flat-flame and atmospheric Bunsen-type stoichiometric CH₄/air premixed flames to evaluate the versatility of the fitting algorithm along with the accuracy and precision of the multi-line NO-LIF thermometry technique.

In the fitting algorithm, the spectral lineshape is fitted with a pseudo-Voigt profile, where the convoluted linewidth and Lorentzian factor are considered. The accuracy of the linewidth fitting is validated through the comparison between the best-fitted linewidths of LIF spectra collected under various sub-atmospheric pressures at room-temperature (~ 290 K) and the corresponding theoretical linewidths. The overall agreement between the best-fitted and estimated linewidths is within 8%. The derived temperatures agree with the thermocouple measurement to within 3%. Additionally, Thermo NO-LIF employs temperature-dependent normalisation term which increases the convergence time of the fitting process by a factor of 10 compared with the conventional method. Thermo NO-LIF, in its current form, is designed to evaluate spectra obtained point-wise. Nonetheless, it can be improved to process imaging measurements in the future. Furthermore, Thermo NO-LIF can be extended to fit excitation spectra of other fluorescence species, provided that the spectroscopic parameters of the species are known. The spectral fitting programme is available to anyone interested in utilising the multi-line NO-LIF thermometry.

The current study demonstrates that, by employing the optimal scan range, high accuracy (0.5%) and precision (4%) can be achieved in a near-adiabatic premixed Bunsen-type flame. It is important to note that, the high standard deviation is due to a small sample size (only three scans because of the long data acquisition duration). The best accuracy and precision occur where scan range B₁ (44303–44341 cm⁻¹) was used. The accuracy and precision decrease slightly with the utilisation of shorter scan ranges (10 and 15 cm⁻¹). The optimal strategy to select a suitable spectral range for multi-line NO-LIF thermometry is to choose a long scan range with least overlapping lines. However, if the experimental condition requires the shortest possible time, the alternative would be to increase the scan rate and to collect more samples to ensure the best accuracy and precision. In this case, a narrowband laser could be a better option than a broadband laser since it provides spectral resolution fine enough to isolate adjacent lines in most cases. Technically, multi-line NO-LIF thermometry requires a minimum of two individual lines to work (similar to the working principle of two-line NO-LIF). Nonetheless, a direct fitting method provides a more robust temperature determination because in addition to the fluorescence peak, the linewidth, which is a function of temperature and pressure, is also considered.

The uncertainty introduced by the overlapping lines might be negligible at sub-atmospheric pressures, but it is a concern at atmospheric pressure. The results also show that while a narrowband laser has the advantage of resolving adjacent transition lines, additional uncertainty

may occur if the resultant spectral linewidth is too narrow. Interestingly, the multi-line NO-LIF thermometry performed with a broadband laser yields a similar performance compared with using a narrowband laser.

5. Acknowledgements

This work is a contribution to the CPER research project CLIMIBIO. The authors thank the French Ministère de l'Enseignement Supérieur et de la Recherche, the Hauts-de-France Region and the European Funds for Regional Economical Development for their financial support to this project.

References

- [1] K. J. Rensberger, J. B. Jeffries, R. A. Copeland, K. Kohse-Höinghaus, M. L. Wise, D. R. Crosley, Laser-induced fluorescence determination of temperatures in low pressure flames, *Applied Optics* 28 (1989) 3556–3566.
- [2] M. Tamura, J. Luque, J. Harrington, P. Berg, G. Smith, J. Jeffries, D. Crosley, Laser-induced fluorescence of seeded nitric oxide as a flame thermometer, *Applied Physics B* 66 (1998) 503–510.
- [3] J. Nygren, J. Engström, J. Walewski, C. Kaminski, M. Aldén, Applications and evaluation of two-line atomic LIF thermometry in sooting combustion environments, *Measurement Science and Technology* 12 (2001) 1294–1303.
- [4] W. Bessler, C. Schulz, Quantitative multi-line NO-LIF temperature imaging, *Applied Physics B* 78 (2004) 519–533.
- [5] A. Denisov, G. Colmegna, P. Jansohn, Temperature measurements in sooting counterflow diffusion flames using laser-induced fluorescence of flame-produced nitric oxide, *Applied Physics B* 116 (2014) 339–346.
- [6] M. D. Sylla, N. Lamoureux, L. Gasnot, Impact of methyl butanoate oxidation on NO formation in laminar low pressure flames, *Fuel* 207 (2017) 801–813.
- [7] A. Hartlieb, B. Atakan, K. Kohse-Höinghaus, Temperature measurement in fuel-rich non-sooting low-pressure hydrocarbon flames, *Applied Physics B* 70 (2000) 435–445.
- [8] R. Devillers, G. Bruneaux, C. Schulz, Development of a two-line OH-laser-induced fluorescence thermometry diagnostics strategy for gas-phase temperature measurements in engines, *Applied Optics* 47 (2008) 5871–5885.
- [9] G. A. Raiche, J. B. Jeffries, Laser-induced fluorescence temperature measurements in a dc arcjet used for diamond deposition, *Applied Optics* 32 (1993) 4629–4635.
- [10] Z. Sun, Z. Alwahabi, B. Dally, G. Nathan, Simultaneously calibrated two-line atomic fluorescence for high-precision temperature imaging in sooting flames, *Proceedings of the Combustion Institute* 37 (2019) 1417–1425.
- [11] J. Borggren, W. Weng, A. Hosseinnia, P.-E. Bengtsson, M. Aldén, Z. Li, Diode laser-based thermometry using two-line atomic fluorescence of indium and gallium, *Applied Physics B* 123 (2017) 278.
- [12] N. Lamoureux, P. Desgroux, A. El Bakali, J. Pauwels, Experimental and numerical study of the role of NCN in prompt-NO formation in low-pressure $\text{CH}_4\text{-O}_2\text{-N}_2$ and $\text{C}_2\text{H}_2\text{-O}_2\text{-N}_2$ flames, *Combustion and Flame* 157 (2010) 1929–1941.
- [13] I. S. McDermid, J. B. Laudenslager, Radiative lifetimes and electronic quenching rate constants for single-photon-excited rotational levels of NO ($A^2\Sigma^+$, $\nu' = 0$), *Journal Quantitative Spectroscopy & Radiative Transfer* 27 (1982) 483–492.
- [14] O. M. Feroughi, H. Kronemayer, T. Dreier, C. Schulz, Effect of fluctuations on time-averaged multi-line NO-LIF thermometry measurements of the gas-phase temperature, *Applied Physics B* 120 (2015) 429–440.

- [15] O. M. Feroughi, S. Hardt, I. Wlokas, T. Hülser, H. Wiggers, T. Dreier, C. Schulz, Laser-based *in situ* measurement and simulation of gas-phase temperature and iron atom concentration in a pilot-plant nanoparticle synthesis reactor, *Proceedings of the Combustion Institute* 35 (2015) 2299–2306.
- [16] H. Kronemayer, P. Ifeacho, C. Hecht, T. Dreier, H. Wiggers, C. Schulz, Gas-temperature imaging in a low-pressure flame reactor for nano-particle synthesis with multi-line NO-LIF thermometry, *Applied Physics B* 88 (2007) 373–377.
- [17] C. Hecht, A. Abdali, T. Dreier, C. Schulz, Gas-temperature imaging in a microwave-plasma nanoparticle-synthesis reactor using multi-line NO-LIF thermometry, *Zeitschrift für Physikalische Chemie* 225 (2011) 1225–1235.
- [18] A. van Gessel, B. Hrycak, M. Jasiński, J. Mizeraczyk, J. van der Mullen, P. Bruggeman, Temperature and NO density measurements by LIF and OES on an atmospheric pressure plasma jet, *Journal of Physics D: Applied Physics* 46 (2013) 095201.
- [19] S. Bejaoui, S. Batut, E. Therssen, N. Lamoureux, P. Desgroux, F. Liu, Measurements and modeling of laser-induced incandescence of soot at different heights in a flat premixed flame, *Applied Physics B* 118 (2015) 449–469.
- [20] C. Betrancourt, F. Liu, P. Desgroux, X. Mercier, A. Faccinetto, M. Salamanca, L. Ruwe, K. Kohse-Höinghaus, D. Emmrich, A. Beyer, A. Gölzhäuser, T. Tritscher, Investigation of the size of the incandescent incipient soot particles in premixed sooting and nucleation flames of *n*-butane using LII, HIM, and 1nm-SMPS, *Aerosol Science and Technology* 51 (2017) 916–935.
- [21] G. M. Watson, P. Versailles, J. M. Berghorson, NO formation in premixed flames of C₁–C₃ alkanes and alcohols, *Combustion and Flame* 169 (2016) 242–260.
- [22] H. Kronemayer, W. Bessler, C. Schulz, Gas-phase temperature imaging in spray systems using multi-line NO-LIF thermometry, *Applied Physics B* 81 (2005) 1071–1074.
- [23] P. C. Palma, P. M. Danchy, A. Houwing, Fluorescence imaging of rotational and vibrational temperature in shock-tunnel nozzle flow, *Journal of AIAA* 41 (2003) 1722–1733.
- [24] J. Luque, D. R. Crosley, Lifbase: Database and spectral simulation program (version 1.5), SRI international report MP 99 (009) (1999).
- [25] W. Bessler, C. Schulz, V. Sick, J. Daily, A versatile modeling tool for nitric oxide LIF spectra, *Proceedings of the Third Joint Meeting of the U.S. Sections of the Combustion Institute* (2003).
- [26] C. M. Western, PGOPHER: A program for simulating rotational, vibration and electronic spectra, *Journal Quantitative Spectroscopy & Radiative Transfer* 186 (2017) 221–242.
- [27] T. Lee, W. G. Bessler, H. Kronemayer, C. Schulz, J. B. Jeffries, Quantitative temperature measurements in high-pressure flames with multiline NO-LIF thermometry, *Applied Optics* 44 (2005) 6718–6728.
- [28] A. Lawitzki, I. Plath, W. Stricker, J. Bittner, U. Meier, K. Kohse-Höinghaus, Laser-induced fluorescence determination of flame temperature in comparison with CARS measurements, *Applied Physics B* 50 (1990) 513–518.
- [29] K. E. Bertagnolli, R. P. Lucht, Temperature profile measurements in stagnation-flow, diamond-forming flames using hydrogen cars spectroscopy, *Proceedings of the Combustion Institute* 26 (1996) 1825–1833.
- [30] F. Grisch, B. Attal-Tretout, A. Bresson, P. Bouchardy, V. Katta, W. Roquemore, Investigation of a dynamic diffusion flame of h₂ in air with laser diagnostics and numerical modeling, *Combustion and Flame* 139 (2004) 28–38.
- [31] A. Bohlin, P.-E. Bengtsson, Rotational CARS thermometry in diffusion flames: On the influence of nitrogen spectral line-broadening by CH₄ and H₂, *Proceedings of the Combustion Institute* 33 (2011) 823–830.
- [32] F. Guichard, P. Boubert, D. Honoré, A. Cessou, CO₂ Spontaneous Raman Scattering: an alternative thermometry for turbulent reactive flows, *International Symposium on the Application of Laser and Imaging Techniques to Fluid Mechanics* 19 (2018).
- [33] A. Lo, G. Cléon, P. Vervisch, A. Cessou, Spontaneous Raman scattering: a useful tool for investigating the afterglow of nanosecond scale discharges in air, *Applied Physics B* 107 (2012) 229–242.
- [34] W. G. Bessler, C. Schulz, T. Lee, J. B. Jeffries, R. K. Hanson, Strategies for laser-induced fluorescence detection of nitric oxide in high-pressure flames III: Comparison of *A-X* excitation schemes, *Applied*

- Optics 42 (2003) 4922–4936.
- [35] C. Schulz, V. Sick, J. Heinze, W. Stricker, Laser-induced-fluorescence detection of nitric oxide in high-pressure flames with $A-X(0,2)$ excitation, *Applied Optics* 36 (1997) 3227–3232.
 - [36] J. R. Reisel, C. D. Carter, N. M. Laurendeau, Einstein coefficients for rotational lines of the (0,0) band of the $\text{NO } A^2\Sigma^+ - X^2\Pi$ system, *Journal of Quantitative Spectroscopy and Radiative Transfer* 47 (1992) 43–54.
 - [37] F. Schreier, The Voigt and complex error function: a comparison of computational methods, *Journal of Quantitative Spectroscopy & Radiative Transfer* 48 (1992) 743–762.
 - [38] F. Schreier, An assessment of some closed-form expressions for the Voigt function II: Utilizing rational approximations for the Gauss function, *Journal of Quantitative Spectroscopy & Radiative Transfer* 202 (2017) 81–89.
 - [39] S. Abrarov, B. Quine, R. Jagpal, A simple interpolating algorithm for the rapid and accurate calculation of the Voigt function, *Journal of Quantitative Spectroscopy & Radiative Transfer* 110 (2009) 376–383.
 - [40] V. Jain, M. C. Biesinger, M. R. Linford, The Gaussian-Lorentzian sum, product, and convolution (Voigt) functions in the context of peak fitting X-ray photoelectron spectroscopy (XPS) narrow scans, *Applied Surface Science* 447 (2018) 548–553.
 - [41] J. F. Kielkopf, New approximation to the Voigt function with applications to spectral-line profile analysis, *Journal of the Optical Society of America* 63 (1973) 987–995.
 - [42] E. Whiting, An empirical approximation to the Voigt profile, *Journal of the Quantitative Spectroscopy & Radiative Transfer* 8 (1968) 1379–1384.
 - [43] F. Schreier, An assessment of some closed-form expressions for the Voigt function, *Journal Quantitative Spectroscopy & Radiative Transfer* 176 (2016) 1–5.
 - [44] F. Schreier, An assessment of some closed-form expressions for the Voigt function III: Combinations of the Lorentz and Gauss functions, *Journal of Quantitative Spectroscopy & Radiative Transfer* 226 (2019) 87–91.
 - [45] E. Whiting, An empirical approximation to the Voigt profile, *Journal of Quantitative Spectroscopy & Radiative Transfer* 8 (1968) 1379–1384.
 - [46] G. Wertheim, M. Butler, K. West, D. Buchanan, Determination of the Gaussian and Lorentzian content of experimental line shapes, *Review of Scientific Instruments* 45 (1974) 1369–1371.
 - [47] J. Olivero, R. Longbothum, Empirical fits to the Voigt line width: a brief review, *Journal of Quantitative Spectroscopy & Radiative Transfer* 17 (1977) 233–236.
 - [48] A. Chang, M. DiRosa, R. Hanson, Temperature dependence of collision broadening and shift in the $A-X(0,0)$ band in the presence of argon and nitrogen, *Journal of Quantitative Spectroscopy & Radiative Transfer* 47 (1992) 375–390.